Nano Research

Open Access

Research Article

MXene-enhanced nanofiber yarns for dual-mode sensing in wearable electronics

Jian Tang[1,2,§], Han Liu[3,§], Yuting Wu[3] ✉, Fatemeh Mokhtari[4], Jizhen Zhang[5], Aldren Ken S. Usman[6], Shidong Ma[3], Tao Yan[3], Zhijuan Pan[3], Chongyi Xu[2], Haibo Xie[1,2], Kaichen Xu[1,2] ✉, Xungai Wang[7], and Joselito M. Razal[7] ✉

[1] *Zhejiang Key Laboratory of Intelligent Manufacturing Industrial Software, Institute of Advanced Machines Zhejiang University, Hangzhou 311100, China*
[2] *State Key Laboratory of Fluid Power and Mechatronic Systems, School of Mechanical Engineering, Zhejiang University, Hangzhou 310058, China*
[3] *National Engineering Laboratory for Modern Silk, College of Textile and Clothing Engineering, Soochow University, Suzhou 215123, China*
[4] *Department of Materials Engineering, KU Leuven, Leuven 3001, Belgium*
[5] *Research Center for Materials Nanoarchitectonics, National Institute for Materials Science (NIMS), Tsukuba 305-0044, Japan*
[6] *Institute for Frontier Materials, Deakin University, Geelong 3216, Australia*
[7] *Joint Research Centre for Fiber Innovations and Renewable Materials, School of Fashion and Textiles, The Hong Kong Polytechnic University, Hong Kong 999077, China*
[§] *Jian Tang and Han Liu contributed equally to this work.*

Cite this article: *Nano Research*, **2026**, *19*, 94908397. https://doi.org/10.26599/NR.2026.94908397

ABSTRACT: Flexible strain-sensing yarns are crucial components in smart textiles. However, integrating high-performance tensile and pressure sensing into a single yarn to monitor comprehensive human activities remains a significant challenge. In this work, we present a dual-model strain-sensing nanofiber yarn fabricated by self-shrinking MXene-coated carbon black/thermoplastic polyurethane (MXene@CB/TPU) composite nanofiber films into Janus-structured slim scrolls, followed by double twisting using internal stress. Carbon black doping enables conductive nanofibers to bridge propagated cracks in MXene coating, forming a synergetic conductive network. This structure enhances the yarn's tensile sensing linearity from 0.810 to 0.994, while achieving a broad range of 106% with a gauge factor of 56. The self-shrunk and double-twisted architecture also provides dual-stage pressure sensitivity, endowing the yarn with an ultrahigh pressure-sensing range of up to 10 MPa, a sensitivity of 17.74 MPa^{-1}, and a linearity of 0.997 (0–3 MPa). Furthermore, the yarn exhibits excellent washability (> 30 ultrasonic washing cycles) owing to crosslinked nanofibers that protect the MXene layer. We demonstrated the practical applicability of this yarn by stitching it into various smart textiles, which successfully detected both tensile and pressure signals from full-range human activities. As a proof-of-concept, a smart waist support developed using this yarn can monitor both dynamic and static waist status. This work achieves high-performance dual tensile and pressure sensing in smart textiles using a single yarn, opening new pathways for advanced wearable electronics.

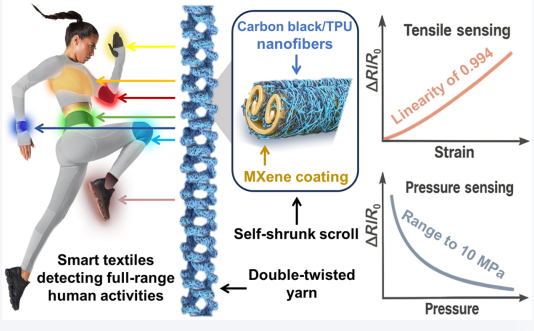

KEYWORDS: flexible tensile/pressure sensor, composite nanofiber yarn, synergetic conductive network, smart textile, human activity monitoring, wearable electronic

1 Introduction

Smart wearable electronics that can monitor and recognize human behaviors are vital for improving health and quality of life [1–5]. Textiles, including clothing, offer a promising platform for next generation of flexible wearable devices due to their inherent softness, body-conforming fit, high coverage, and versatile structural and functional design potential [6–10].

Yarn-based flexible strain sensors, which can be knitted, woven, or stitched into fabrics, serve as essential sensing components in smart textiles. These sensors convert body movements into electrical signals [11–15]. Coating elastic fibers with conductive

Received: November 11, 2025; **Revised:** December 25, 2025
Accepted: December 31, 2025

✉Address correspondence to Joselito M. Razal, joselito.razal@polyu.edu.hk; Kaichen Xu, xukc@zju.edu.cn; Yuting Wu, ytwu@suda.edu.cn

layers remains one of the most effective approaches for producing high-performance resistive yarn sensors [16–19]. However, several challenges hinder their practical applications. First, the preparation process is often complex, typically requiring multiple steps, such as multilayer coating and surface modification, to improve the thickness and adhesion of the conductive layer [20–24]. Second, yarn sensors with high aspect ratios are primarily sensitive to tensile strain and exhibit limited responsiveness to other deformation types, especially pressure. Their small cross-sectional size and restricted radial deformation range further constrain pressure-sensing performance. A common solution is to assemble multiple conductive yarns into intersecting structures, where overlapping points act as pressure-sensitive units based on contact resistance changes [25–28]. Our group previously developed machine-knitted strain-sensing nanofiber yarns to create fabric sensors with anisotropic tensile and pressure sensitivity [29]. Nevertheless, achieving a wide pressure sensing range using a single yarn remains challenging [30]. Third, conductive coatings exposed to the environment are susceptible to peeling and damage, compromising the washability and durability of yarn sensors [31–33]. While adding a protective overcoat can mitigate this issue [23], such encapsulation complicates manufacturing, alters sensing behavior unpredictably, and introduces challenges in electrode integration.

In this work, we fabricated a washable, high-performance tensile and pressure-sensing yarn from MXene-coated carbon black/thermoplastic polyurethane (MXene@CB/TPU) composite nanofibers using a facile process. The fabrication began with the preparation of a CB/TPU composite nanofiber film via double-needle *in-situ* electrospinning, producing a blend of TPU nanofibers and CB-doped TPU nanofibers. A Janus-structured MXene@CB/TPU film was then created by scrape-coating MXene onto this base. Subsequently, the films were self-shrunk into scrolls using a solvent and spontaneously entangled into a double-twisted yarn driven by internal stress. The MXene loading and CB-doped TPU nanofiber proportion were optimized based on the mechanical, conductive, and sensing properties of the resulting yarns. We comprehensively evaluated the MXene@CB/TPU yarn's sensing performance, including its ranges, sensitivity, linearity, and durability under both tensile and pressure stimuli. The enhancement mechanism was attributed to the synergetic MXene/nanofiber conductive network and the unique self-shrunk/double-twisted yarn structure. Finally, we demonstrated the yarn's practical applicability by integrating it into various smart textiles. A single sensing yarn successfully monitored human motions, physiological signals, and tactile pressures. Notably, we developed a smart waist support belt capable of detecting both static and dynamic waist status.

2 Experimental section

2.1 Materials

CB (code XFI15; grain size = 23 nm) was provided by Nanjing XFNANO Materials Tech Co., Ltd. The nanocarbon dispersant (code C139963; a hydrophobically modified poly(vinyl alcohol) product) was supplied by Aladdin Industrial Co., Ltd. TPU (code 1195A) was sourced from BASF Co., Ltd. N,N-dimethylformamide (DMF; ≥ 99.0%) and tetrahydrofuran (THF; ≥ 99.5%) were obtained from Sinopharm Group Chemical Reagent Co. Ltd. The MXene ink consisted of an aqueous dispersion of single-layer MXene prepared from MAX phase using the minimally intensive layer delamination method [34–36] and its characteristics are shown in Fig. S1 in the Electronic Supplementary Material (ESM).

2.2 Preparation of CB/TPU composite nanofiber film

The nanocarbon dispersant (20 wt.% relative to CB) was dissolved in a DMF/THF mixed solvent (1:1 mass ratio). CB particles (30 wt.% of solute) were then dispersed in this solvent via 1 h ultrasonication. TPU grains (9 wt.% of the total solution) were subsequently dissolved into the CB dispersion under 12 h of stirring to obtain a uniform CB-doped TPU solution.

CB/TPU composite nanofiber films were fabricated by double-needle *in-situ* electrospinning, simultaneously depositing pure TPU nanofibers and CB-doped TPU nanofibers onto an aluminum foil collector (Fig. 1(a)). The feeding rate of the TPU solution was maintained at 4 mL/h, while the feeding rate of the CB-doped TPU solution was adjusted to control the ratio of pure to CB-doped nanofibers. The inner diameter of the spinning needles was 0.41 mm, the applied voltage was 20 kV, and the distance from the needle tip to the drum collector was 22 cm. The drum collector (diameter: 26 cm) was rotated at a speed of 20 m/min.

2.3 Preparation of MXene@CB/TPU composite nanofiber yarn

The electrospun sample was cut into 1 cm wide strips. The MXene ink was then scrape-coated onto the CB/TPU composite nanofiber film using a Mayer rod coating method [37–39], followed by a drying step (Fig. 1(b)). The MXene ink loading was controlled at 5 mg/cm^2.

Next, the MXene@CB/TPU composite nanofiber film was wetted with an 80% DMF aqueous solution (Fig. 1(c)) and easily peeled from the aluminum foil (Fig. 1(d)). After separation, the film self-shrank into a slim scroll-like shape and was subsequently dried (Fig. 1(e)). This bionic process simulated the upward curling of leaves to protect water from evaporation when plants were subjected to drought conditions (Fig. S2 in the ESM).

Afterwards, two scrolls were combined and carried out to a first twisting process to 2000 twists/m (Fig. 1(f)). The initially twisted scrolls were then folded with a weight suspended at the midpoint and underwent double twisting in the reverse direction until the internal stress from the first twisting was fully released (Fig. 1(g)). This process formed a MXene@CB/TPU composite nanofiber yarn with a double-twisted structure without requiring any post-treatment.

2.4 Characterization

The morphologies of the samples were characterized using cold field-emission scanning electron microscopy (SEM; Jeol NeoScope JCM-5000), transmission electron microscopy (TEM; Hitachi HT7700), and atomic force microscopy (AFM; Bruker MM8). The corresponding elemental distributions were obtained by energy dispersive spectroscopy (EDS; Oxford UlLTIM MAX 40). Crystal structures were analyzed with an X-ray diffractometer (XRD; Bruker D8 Advance). Water contact angles were measured five times per sample using a contact angle goniometer (Chengde Dingsheng JY-82C). Mechanical properties were evaluated through ten tests on a universal testing machine (Instron 5967) at a test speed of 500 mm/min and a gauge length of 500 mm.

To evaluate the sensing performance of the yarns, tensile and pressure stimuli were applied using a universal testing machine

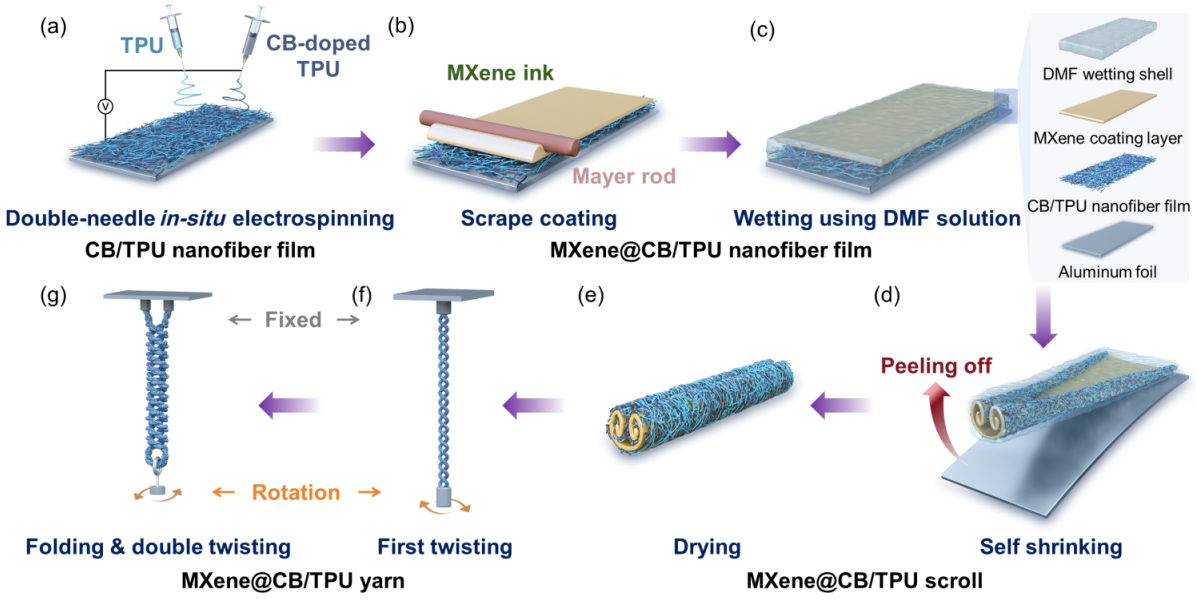

Figure 1 Flowchart illustrating the preparation of MXene@CB/TPU composite nanofiber yarn: (a) double-needle *in-situ* electrospinning of the CB/TPU composite nanofiber film; (b) scrape-coating of MXene onto the CB/TPU composite nanofiber film; (c) wetting and (d) self-shrinking MXene@CB/TPU composite nanofiber film; (e) schematic diagram of the MXene@CB/TPU composite nanofiber scroll; and preparation processes of the MXene@CB/TPU composite nanofiber yarn after (f) first twisting and (g) double twisting.

(Instron 5967), while a digital multimeter (Keysight 34461A) recorded the real-time resistance. Ultrasonic washing tests were performed in deionized water; each 5 min wash cycle used an ultrasonic power of 300 W.

3 Results and discussion

3.1 Morphologies of nanofiber film, scroll, and yarn

The double-needle *in-situ* electrospun CB/TPU composite nanofiber film is shown in Fig. 2(a). The film consisted of a randomly interwoven network of CB-doped TPU nanofibers (20 wt.%) and pure TPU nanofibers (80 wt.%), with average diameters of 1805 ± 473 and 941 ± 230 nm, respectively. While the TPU nanofibers exhibited smooth surfaces, the SEM and TEM images (Fig. 2(b)) show that CB particles are dispersed within the composite nanofibers and partially exposed on the fiber surface, forming conductive networks across the nanofiber matrix. After scrape-coating 1 wt.% MXene solution, single-layer MXene nanosheets adhered conformally and stacked evenly on the nanofiber film surface, forming a continuous conductive coating layer (Fig. 2(c)). The EDS mapping of Ti element distribution (Fig. 2(d)) confirms that MXene nanosheets are uniformly distributed throughout the coating. The cross-sectional morphology (Fig. 2(e)) further reveals that the MXene ink forms a continuous film layer with a thickness of 350 ± 49 nm on top of the nanofiber mat (7.35 ± 0.78 μm thick), rather than conformally coating individual fibers.

Not all solvents had fully evaporated from the nanofibers immediately upon reaching the drum collector. Consequently, the bottom nanofibers, those in direct contact with the aluminum foil, formed clumps after complete solidification (Fig. 2(f)). In contrast, subsequently deposited nanofibers were cylindrical, with diameters less than half of those at the bottom, and possessed higher internal stress. This stress differential caused both edges of the film to spontaneously curl upward and roll inward upon separation from the aluminum foil. This curling behavior was further driven by asymmetric wettability. The top MXene-coated surface was highly hydrophilic (water contact angle: 51°), while the bottom nanofiber film was more hydrophobic (water contact angle: 122°) (Fig. S3 in the ESM). After wetting, the hydrophilic top surface retained more solution, and the combined effects of stronger hydrogen bonding forces and surface tension promoted the observed shrinking.

Consequently, when wetted with a DMF aqueous solution and separated from the aluminum foil, the Janus structured MXene@CB/TPU composite nanofiber film self-shrunk into a slim scroll (Fig. 2(g)). During this process, the two edges of the film curled inward, made contact, and sealed. After drying, the nanofibers crosslinked into an integrated structure that encapsulated and protected the internal MXene layer. This scroll exhibited a more compact structure than one formed using deionized water, which contained obvious internal pores (Fig. 2(h)). The compactness arises because DMF, a good solvent for TPU, causes swelling and slight dissolution of the nanofiber surface, effectively acting as an adhesive during shrinking.

Twisting is a standard method for converting nanofiber films into yarns suitable for further processing [40–42]. However, this process induces internal stress, which typically requires post-setting treatments, often under prolonged high temperature and humidity, to achieve a stable structure. These conditions are highly detrimental to conductive MXene materials [43]. In this work, we introduced an alternative approach. The initially twisted scrolls were folded in half, harnessing their internal stress to drive a second self-twisting motion. This formed a double-twisted yarn structure with a diameter of 519 ± 34 μm (Fig. 2(i)). During twisting, the scrolls underwent stretching, which aligned the nanofibers slightly along the scroll axis. This alignment further wrapped and protected the inner MXene coatings.

3.2 Effect of MXene concentrations on properties of nanofiber yarn

As a highly conductive two-dimensional nanomaterial, MXene can

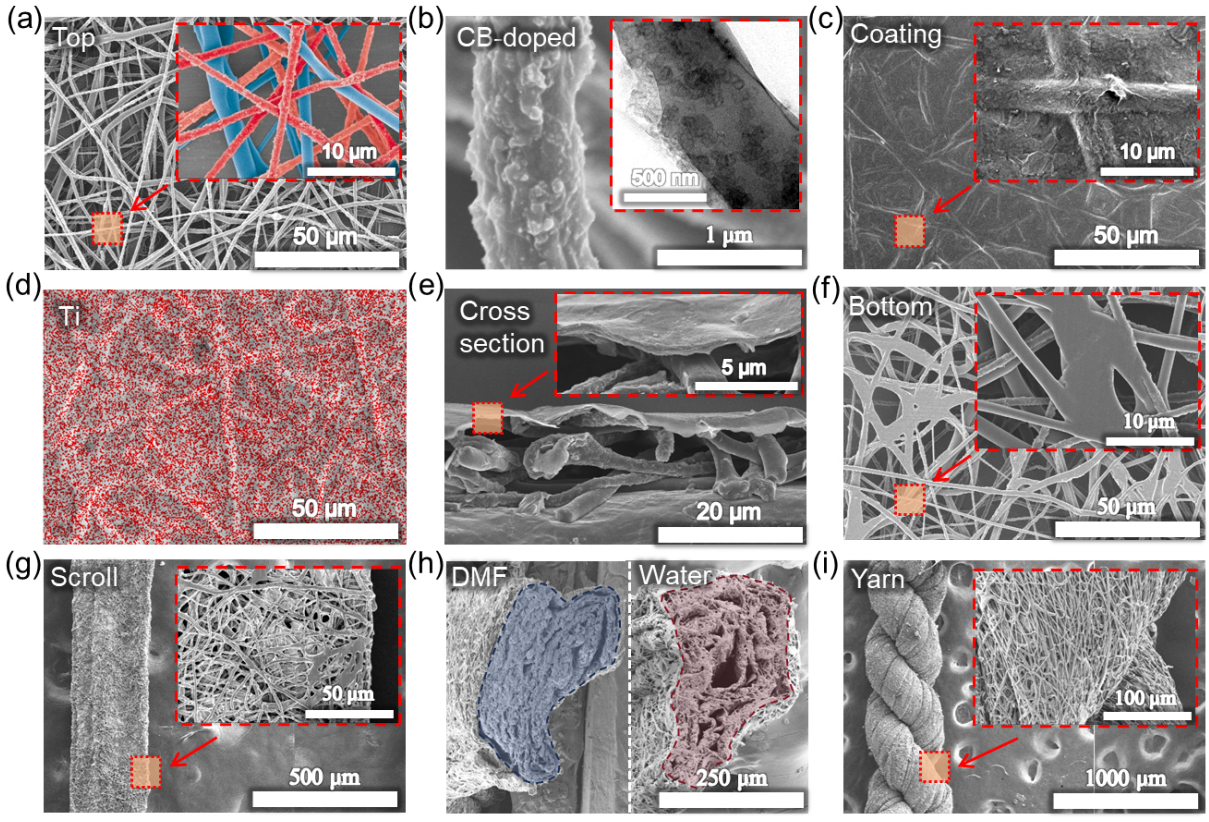

Figure 2 SEM, TEM, and EDS images of the composite materials: (a) CB/TPU composite nanofiber film (inset shows pure TPU nanofibers dyed blue and CB-doped TPU nanofibers dyed red); (b) CB-doped TPU nanofibers; (c) MXene@CB/TPU composite nanofiber film; (d) Ti element distribution in the coating layer; (e) cross-section of (c); (f) back side of (a); (g) MXene@CB/TPU composite nanofiber scroll; (h) cross-sections of MXene@CB/TPU composite nanofiber scrolls self-shrunk using a DMF aqueous solution and deionized water; and (i) MXene@CB/TPU composite nanofiber yarn.

be coated onto elastic polymer substrates to create resistive flexible strain sensors [44–46]. This study investigated the influence of MXene loading on the properties of MXene@TPU composite nanofiber yarn (without CB doping) by adjusting the MXene ink concentration during the scrape-coating process (Figs. 3(a)–3(c)).

A mechanical mismatch between the MXene coating and the TPU nanofibers caused some MXene flakes that penetrated the network's voids to hinder nanofiber alignment and slippage. Consequently, as MXene loading increased, the yarn's breaking elongation decreased while its breaking stress rose (Fig. 3(a)). However, when the ink concentration exceeded 2 wt.%, excessive MXene wrapped within the yarn significantly deteriorated its mechanical properties.

Thicker MXene coating substantially reduced yarn resistivity. Notably, increasing the MXene concentration from 0.5 wt.% to 1 wt.% caused a sharp drop in resistivity from 532 to 207 kΩ/cm (Fig. 3(b)). This occurred because the 1 wt.% concentration produced a continuous, uniform conductive layer (Fig. 2(b)), whereas the 0.5 wt.% coating contained gaps (Fig. S4 in the ESM). Further thickening the MXene coating had a diminished effect on conductivity, as the internal MXenes were separated from external electrodes by the nanofiber layer.

Figure 3(c) shows the relative resistance change (RRC)–strain curves of yarns prepared with different MXene concentrations. The slope of the curves represents the strain-sensing sensitivity, defined as the gauge factor (GF) [47]. A thin MXene layer, operating on a "crack mechanism" [48], was too brittle. It generated drastic RRC at small strains but broke under large strains, yielding unstable responses. A thicker coating maintains continuity under larger strains, expanding sensing range but reducing sensitivity. Excessive thickness caused a deformation mismatch between the rigid MXene layer and elastic nanofibers, leading to severe fluctuations and unstable sensing. Therefore, 1 wt.% was identified as the optimal MXene ink concentration. At this loading, the MXene@TPU yarn achieved a maximum detectable strain of 66.4% with high sensitivity (GF = 423.9), albeit with limited linearity (R^2 = 0.810).

3.3 Effect of CB-doped TPU nanofiber proportions on properties of nanofiber yarn

Low linearity in strain sensors complicates the relationship between input strain and output signals, hindering practical application. Typically, complex structural designs are required to regulate the disconnection rate of the conductive coatings, which accelerates under increasing strain [49–51]. In this work, we optimized the sensing performance of the MXene@TPU composite nanofiber yarn through a simple approach: partially replacing insulating TPU nanofibers with conductive CB-doped TPU nanofibers using a double-needle *in-situ* electrospinning process. This modification collaboratively constructed a synergetic conductive network with the MXene coating, significantly improving sensing linearity.

Based on our previous work investigating the effects of filler content and dispersion states on the properties of CB-doped TPU nanofibers [11, 12], 30 wt.% CB and a poly(vinyl alcohol) dispersant dosage of 20 wt.% relative to the CB mass was identified as the optimal formulation to achieve a favorable balance between mechanical performance and electrical conductivity. Compared to

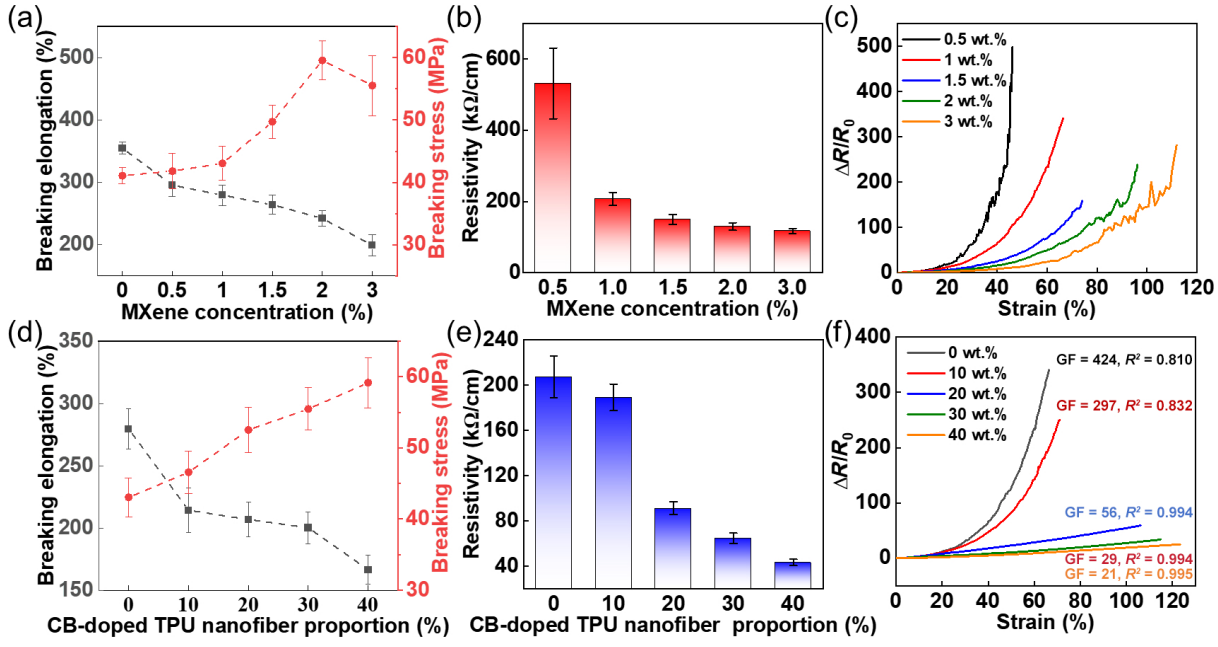

Figure 3 Characterization of MXene@TPU composite nanofiber yarns (without CB doping) prepared with MXene inks at different concentrations: (a) breaking elongation and stress, (b) resistivity, and (c) RRC–strain curves. Characterization of MXene@CB/TPU composite nanofiber yarns prepared with 1 wt.% MXene ink and different proportions of CB-doped TPU nanofibers: (d) breaking elongation and stress, (e) resistivity, and (f) RRC–strain curves.

purely insulating TPU nanofiber yarn, yarns made entirely from CB-doped TPU nanofibers exhibited high conductivity but poor elasticity, with resistivity dropping to 23 kΩ/cm, breaking stress increasing by 115%, and breaking elongation decreasing by 61%. Therefore, partially replacing TPU nanofibers with conductive ones offers a more balanced solution.

Figures 3(d) and 3(e) show the mechanical and conductive properties of MXene@CB/TPU yarns (using 1 wt.% MXene ink) with varying proportions of CB-doped TPU nanofibers. Increasing the conductive nanofiber proportion enhanced yarn strength and conductivity but reduced stretchability. Notably, when the percentage increased from 10 wt.% to 20 wt.%, resistivity sharply decreased from 189 to 91 kΩ/cm (Fig. 3(e)). This suggests that at 20 wt.%, a dual conductive network is achieved: The conductive nanofibers not only reinforce the MXene coating but also interweave to form an independent, continuous conductive pathway. The synergy between these two networks substantially improved electron transport capability.

Increasing the proportion of CB-doped TPU nanofibers expanded the strain sensing range of the MXene@CB/TPU yarn but reduced its sensitivity (Fig. 3(f)). This trade-off occurred because the one-dimensional conductive nanofibers bridged cracks within the two-dimensional MXene coating during stretching. This maintained the continuity of the synergetic conductive network under larger strains, thereby dampening the overall resistance change.

Critically, at a 20 wt.% conductive nanofiber proportion, the dual conductive networks generated a synergistic effect on resistance response, dramatically improving R^2 to 0.994. Beyond this point, further increases in the conductive nanofiber proportion only marginally improved linearity and the maximum detectable strain, while sensitivity continued to decline. Consequently, 20 wt.% was selected as the optimal proportion. At this ratio, the MXene@CB/TPU yarn achieved a remarkable sensing range of 106% and a GF of 56. This performance meets the requirements for smart textile applications and surpasses that of many recently reported yarn-based resistive strain sensors with good linearity (Fig. 4(a)) [33, 52–57].

3.4 Tensile-sensing performance of nanofiber yarn

Figure 4(b) displays the RRC curves for the MXene@TPU yarn, MXene@CB/TPU scroll, and MXene@CB/TPU yarn during the first 20 cycles of a 50% cyclic tensile strain test. The resistance response peaks for all three sensors gradually decreased with increasing cycle number. However, introducing conductive CB-doped TPU nanofibers significantly improved dynamic drift and repeatability. The decline in resistance peaks over 20 cycles dropped from 49.1% to 6.8%, while the coefficient of variation (CV) for resistance peaks in the last five cycles decreased from 4.4% to 0.7%, demonstrating the superior stability of the synergetic conductive network. Additionally, the untwisted scroll showed higher dynamic drift (65.1%) and a CV for peak of 1.6%. The enhanced stability of the twisted yarn is attributed to the increased conductive pathways from combining four scrolls and the pre-stretching [58] of the network during twisting.

The MXene@CB/TPU yarn accurately detected cyclic tensile strains from 0.1% to 100% (Fig. 4(c)). During cyclic stress–strain loading (Fig. 4(d)), the yarn with a double-twisted, self-shrunk scroll structure exhibited no pronounced mechanical hysteresis or stress softening, which underpins its stable tensile-sensing behavior. Under cyclic strains of the same amplitude, the peak resistance remained consistent across different stretching speeds (Fig. S5 in the ESM). However, the baseline resistance increased due to reduced elastic recovery of the polymer substrate, leading to a slight decrease in RRC peaks (Fig. 4(e)). In the quasi-static step strain tests, the yarn exhibited excellent static stability with minimal resistance drift (Fig. 4(f)). The response times for stretching and releasing were 180 and 230 ms, respectively.

During a 5000-cycle durability test at 50% strain, the yarn showed a low resistance drift rate of 10% with virtually unchanged

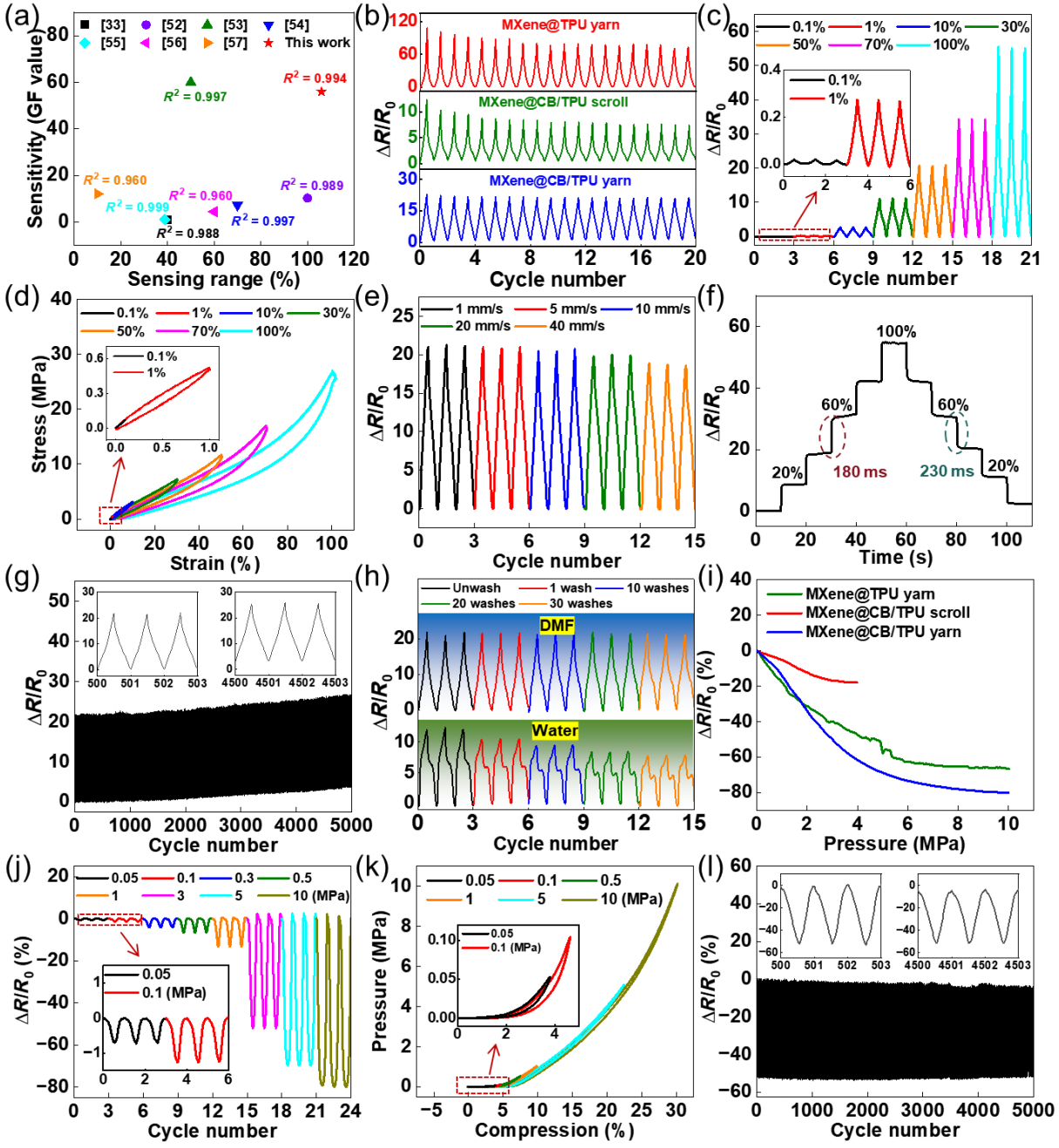

Figure 4 Dual-mode sensing performance of the composite yarns. (a) Comparison of the tensile sensing range, sensitivity, and linearity between the MXene@CB/TPU yarn and recently reported yarn-based strain sensors with good linearity. (b) RRC of MXene@TPU yarn, MXene@CB/TPU scroll, and MXene@CB/TPU yarn during the first 20 cycles of a 50% cyclic tensile strain test. Tensile sensing performance of the MXene@CB/TPU yarn: (c) RRC under different cyclic strain amplitudes; (d) stress–strain curves corresponding to (c); (e) RRC under various strain rates; (f) RRC under quasi-static step strain from 0% to 100%, including response times; and (g) RRC during 5000 cycles of 50% strain. (h) RRC of MXene@CB/TPU yarns self-shrunk in DMF aqueous solution and deionized water under 50% cyclic strain after different numbers of ultrasonic washing cycles. (i) RRC–pressure curves of MXene@TPU yarn, MXene@CB/TPU scroll, and MXene@CB/TPU yarn. Pressure sensing performance of the MXene@CB/TPU yarn: (j) RRC under different cyclic pressure amplitudes; (k) pressure–compression curves corresponding to (j); and (l) RRC during 5000 cycles at 3 MPa pressure.

signal characteristics, highlighting the robustness of the self-shrunk scroll and double-twisted yarn structures (Fig. 4(g)). Furthermore, after over 30 ultrasonic washing cycles, the yarn formed with DMF aqueous solution retained its sensing performance, while the yarn made with deionized water degraded significantly (Fig. 4(h)). This excellent washability is attributed to DMF-assisted crosslinking of the nanofiber film, which effectively prevents MXene leakage (Fig. S6 in the ESM). The crosslinked nanofibers also form a robust framework, yielding superior linear and sensitive resistance responses under cyclic strain compared to yarns shrunk in deionized water.

3.5 Pressure-sensing performance of nanofiber yarn

The contact pressure between the human body and external objects can exceed 5 MPa [59]. The MXene@CB/TPU composite nanofiber yarn, with its self-shrunk and double-twisted structures, could

detect pressures up to 10 MPa. It demonstrated a sensitivity of 17.7 MPa^{-1} and a linearity of 0.997 within the 0–3 MPa range (Fig. 4(i)). Moreover, the yarn exhibited repeatable single-peak negative resistance responses to cyclic pressures ranging from 0.05 to 10 MPa (Fig. 4(j)), along with negligible mechanical hysteresis during pressure loading–unloading cycles (Fig. 4(k)). It also showed excellent durability over 5000 cycles at 3 MPa (Fig. 4(l)), demonstrating its outstanding dynamic pressure-sensing performance.

The pressure-sensing signal of the MXene@TPU yarn exhibited significant fluctuations (Fig. 4(i)), resulting from the random contact and separation of the conductive MXene coating across the porous insulating TPU nanofiber membrane. In contrast, MXene@CB/TPU yarn, featuring a synergetic conductive network, showed significantly improved linearity, stability, and sensitivity. This enhancement is attributed to the additional conductive pathways provided by the CB/TPU nanofibers under compression. Additionally, the untwisted MXene@CB/TPU scroll had a limited maximum detectable pressure of less than 4 MPa and a lower sensitivity of 5 MPa^{-1}. This comparison indicates that the double-twisted structure greatly improves pressure sensing performance by enhancing contact resistance variation between scrolls.

3.6 Tensile and pressure-sensing mechanism of nanofiber yarn

Based on SEM observations of the structural evolution of the MXene@CB/TPU composite nanofiber film under stretching (Figs. 5(a) and 5(b)), we propose a tensile-sensing mechanism for the synergetic conductive network (Fig. 5(c)). In the initial state, electrons are transmitted primarily through the highly conductive MXene coating. Under strain, cracks first propagate perpendicular to the strain direction in the high-modulus MXene layer and then expand along the nanofiber network (Figs. 5(a) and 5(c)). At small strains, this "crack effect" [48] is the primary mechanism responsible for the tensile-sensing behavior.

However, excessive crack propagation causes abrupt resistance changes and nonlinear response signals. To address this, the conductive CB-doped nanofiber network bridges these cracks (Figs. 5(b) and 5(c)), slowing the disconnection rate of the conductive network and providing exceptional sensing linearity. As stretching continues, the slightly aligned conductive nanofibers and the fractured MXene layers form an "island-bridge" architecture. At this stage, electrons flow primarily through the CB-doped nanofiber network, while the MXene islands enhance the overall conductivity, thereby expanding the tensile sensing range.

To elucidate the contact interactions within the multilayer architecture of the yarn under pressure, and thereby provide insight into its pressure-sensing mechanism, a simplified finite element model (FEM) was constructed (Fig. 5(d)). The cross-section of a self-shrunk scroll was idealized as a set of concentric rings, representing alternating nanofiber and MXene layers wrapped in a layer-by-layer manner. The double-twisted yarn was further simplified as two

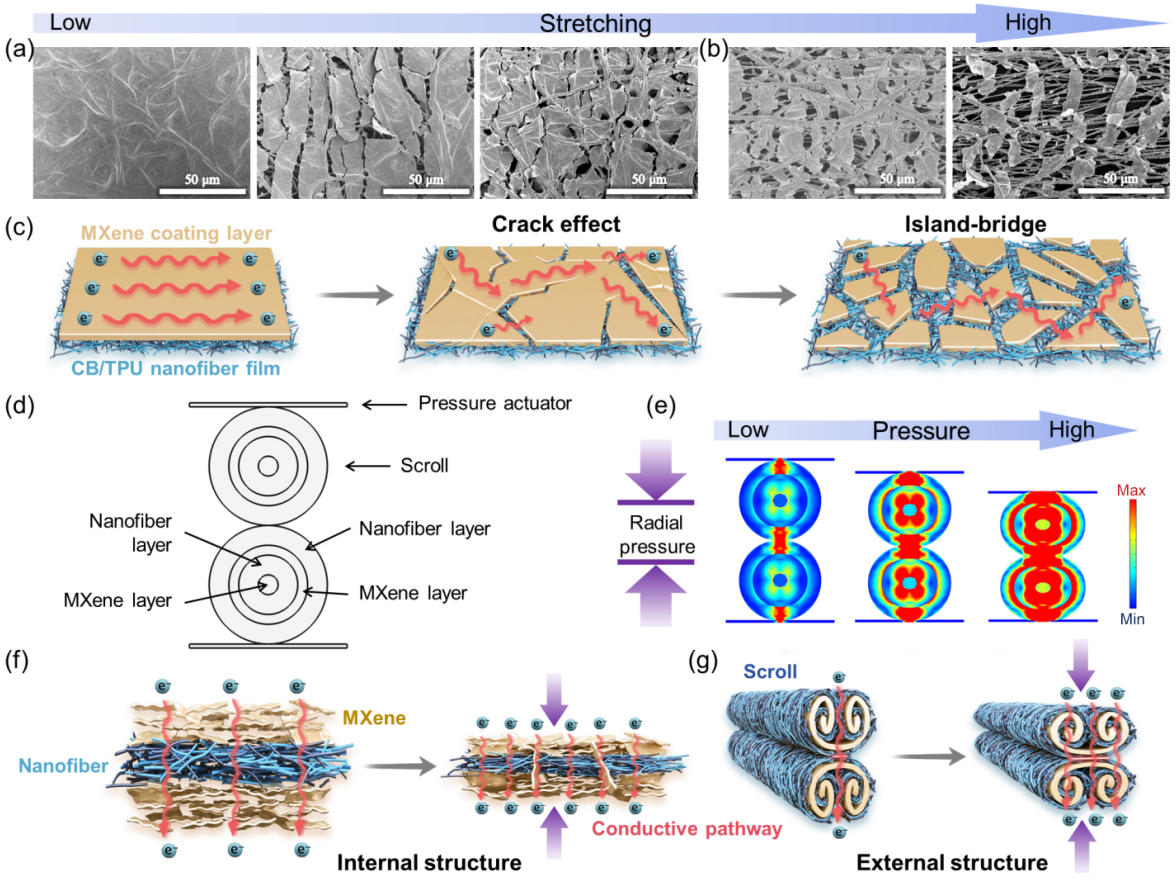

Figure 5 Mechanistic analysis of the MXene@CB/TPU yarn. SEM images of the MXene@CB/TPU film under (a) small and (b) large strain levels. (c) Schematic illustrating the tensile sensing mechanism of the synergetic conductive network in the yarn. (d) Specifications of the FEM model for the MXene@CB/TPU yarn. (e) FEM simulation showing the equivalent stress distribution on yarn model under increasing radial pressure. Pressure-sensing mechanism of the MXene@CB/TPU yarn: (f) internal and (g) external yarn structures.

such scrolls stacked in parallel. By applying increasing radial pressures using a flat-plate actuator and calculating the equivalent stress distribution across the yarn cross-section (Fig. 5(e)), the FEM simulation indicates that the contact force increases at two key interfaces: between the nanofiber layer and the MXene layer within each scroll, and between adjacent scrolls.

The pressure-sensing behavior of the yarn is primarily attributed to variations in its cross-sectional structure and radial resistance. Based on the experimental and simulation results above, we established a dual-stage pressure-sensing mechanism (Figs. 5(f) and 5(g)). In the internal stage (Fig. 5(f)), the nanofiber films serve as piezoresistive layers sandwiched between MXene coatings within the multilayer framework. Under increasing pressure, the elastic nanofiber film is compressed, allowing more MXene on opposite sides to make contact through the pores of the nanofiber network and thereby creating additional interlayer conductive pathways. Meanwhile, the enhanced contact force between adjacent MXene nanosheets decreases the intrinsic resistance of the coatings. In addition, introducing CB-doped nanofibers creates more piezoresistive units, including contact-resistance variations at the interfaces between conductive nanofibers and the coating, as well as among interwoven conductive nanofibers, thereby improving the magnitude and consistency of the overall piezoresistive response. In the external stage (Fig. 5(g)), the double-twisted yarn structure increases the contact area and force between conductive scrolls under pressure, consequently diminishing contact resistance according to Holm's theory [60]. The synergy between these internal and external mechanisms enables the ultra-wide pressure-sensing range of the MXene@CB/TPU yarn.

3.7 Smart textile application

To validate its application in smart textiles, a 2 cm long MXene@CB/TPU yarn was integrated into fabrics using self-locking stitches [61], complemented with microelectrodes and stretchable interconnects [29]. The yarn was embedded into a kneepad, elbow pad, and wristband, where it effectively monitored the bending amplitudes and frequencies of the corresponding joints (Figs. 6(a)–6(c)). During these large joint movements, the yarn exhibited a unimodal positive RRC.

When incorporated into elastic bandages wrapped around the chest and abdomen, the same yarn detected subtle deformations from heartbeat and respiration, measuring 85.7 bpm and

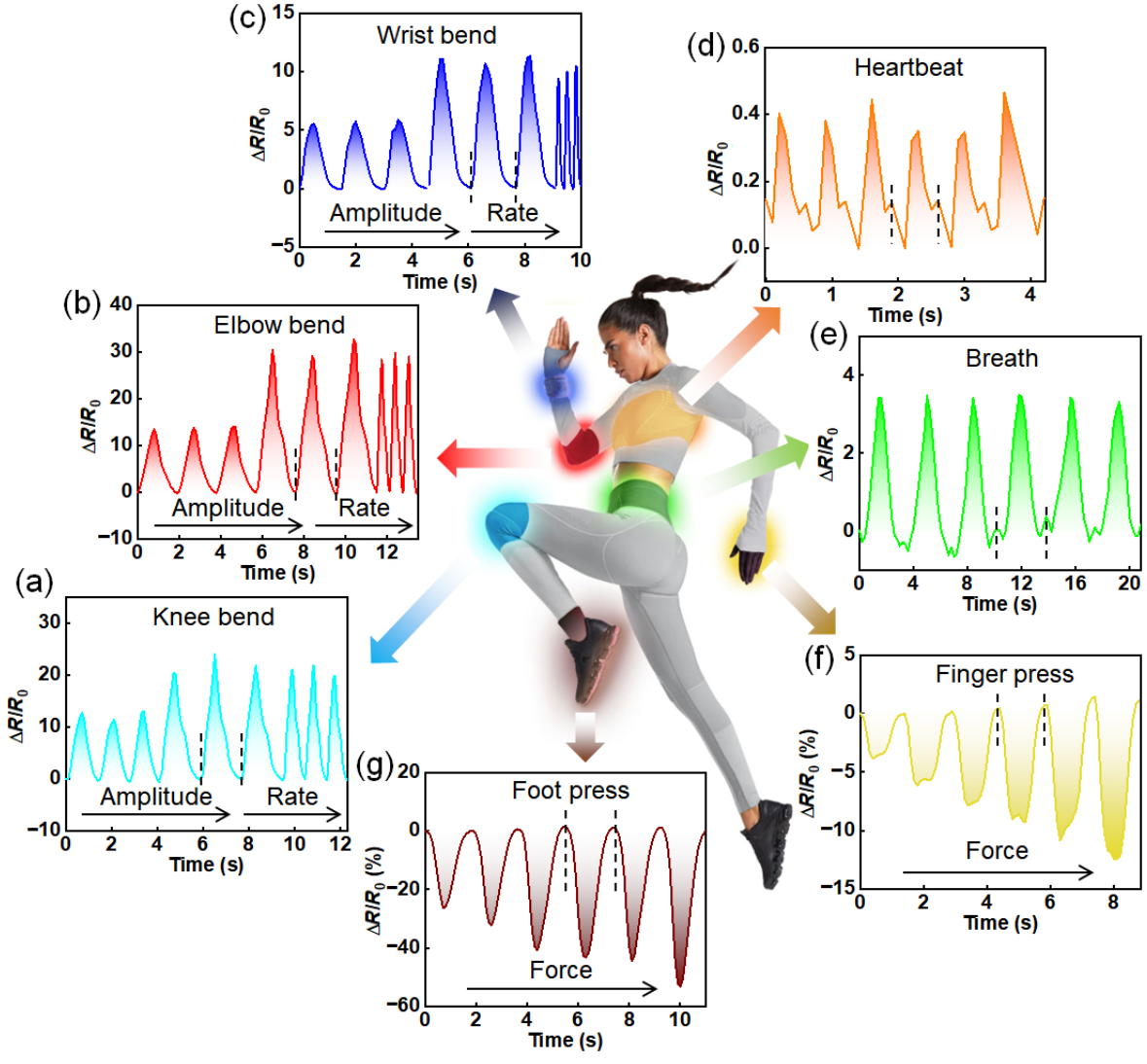

Figure 6 RRC of the MXene@CB/TPU yarn stitched into textiles for monitoring: (a) knee bending, (b) elbow bending, (c) wrist bending, (d) heartbeat, (e) breathing, (f) finger pressing, and (g) foot pressing.

17.3 cycles/min, respectively, in this test (Figs. 6(d) and 6(e)). Remarkably, in gloves and socks, the yarns demonstrated negative piezoresistive responses during finger-object interactions and footstep pressures, with signal amplitudes proportional to the applied force (Figs. 6(f) and 6(g)).

Lower back pain is a highly common condition, and waist supports can protect the waist and assist in rehabilitation. We developed a smart, self-adhesive waist support belt with a sensing yarn embedded parallel to the fabric at its core (Fig. S7 in the ESM). This belt monitors forces exerted on the waist during physical activity, providing valuable data for pain management and posture correction.

We demonstrate the belt's functionality across various movements. During walking, the belt stretches and produces a positive RRC (Fig. 7(a)). Significant twisting motions generate stronger responses (Fig. 7(b)). Therefore, by alerting users to walking duration and the degree of waist twisting, the belt can help prevent muscle fatigue. Conversely, bending motions increase pressure on the waist. This "bend over" movement causes the belt to exhibit a negative piezoresistive response, with the signal intensifying as the bending angle increases (Fig. 7(c)). Our data show that squats and jumps subject the waist to distinct pressure profiles (Figs. 7(d) and 7(e)). Therefore, this belt can enable patients to monitor the duration, intensity, and frequency of pressure exerted on their waists during daily activities. These functionalities enable timely adjustments to various movements to mitigate strain and support recovery.

Incorrect sitting postures, such as excessive forward or backward leaning, impose severe strain on the lumbar spine and surrounding muscles. Application results in Fig. 7(f) confirm that when a volunteer changed from standing to sitting with an upright posture, the resistive signal from the smart belt decreased, reflecting the increased pressure on the sensing yarn. This occurs because sitting shifts the body's center of gravity backward, amplifying compressive forces on the lumbar spine compared to standing [62].

Notably, a backward-leaning posture further reduced the resistance signal, indicating even higher-pressure levels. Conversely, reverting to proper posture immediately restored the signal baseline. Furthermore, a forward-leaning posture exerted greatest pressure due to the absence of backrest support. These findings are consistent with actual anthropometric data [63]. When the user returned to a standing position, the resistance signal recovered to nearly its initial baseline, demonstrating the reliable recovery capability of the smart belt.

When the body maintained a static posture, the smart belt's sensor signal showed excellent stability (Fig. 7(f)). The minor signal fluctuations observed were motion artifacts caused by abdominal breathing; their intensity was negligible compared to the response generated by postural changes. Therefore, this smart waist support belt can effectively warn users who remain in an incorrect sitting posture for extended periods and assist in posture correction.

In summary, a single MXene@CB/TPU yarn, sensitive to both tensile and pressure, can be stitched into various textiles. This enables the collaborative monitoring of large-scale human motion, subtle physiological activities, and external contact pressure. Integrated into a waist support belt, the yarn successfully monitored

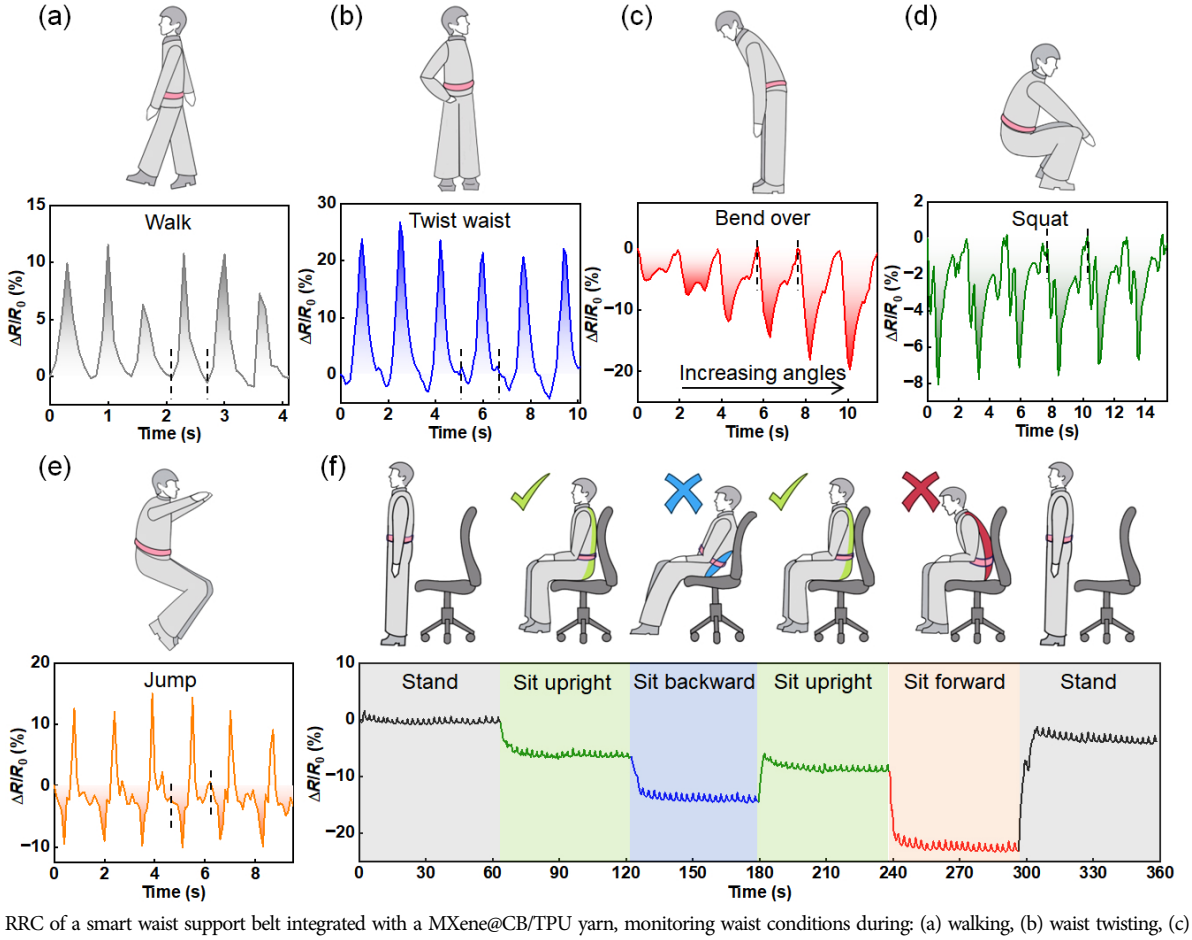

Figure 7 RRC of a smart waist support belt integrated with a MXene@CB/TPU yarn, monitoring waist conditions during: (a) walking, (b) waist twisting, (c) bending over with increasing angles, (d) squatting, (e) jumping, and (f) different sitting positions.

dynamic waist pressure during activity and identified lumbar pressure changes caused by static sitting postures. These results demonstrate the significant potential of the MXene@CB/TPU yarn for all-around human signal monitoring in smart textiles.

4 Conclusions

This work developed a high-performance nanofiber yarn capable of sensing both tension and pressure through the construction of a MXene-based synergetic conductive network and a uniquely designed self-shrinking, double-twisted structure. Janus-structured MXene@CB/TPU films self-shrunk into scrolls with the assistance of a DMF aqueous solution, enabling elastic nanofiber webs to encapsulate conductive MXene coatings layer by layer. The scrolls then spontaneously entangle into stable double-twisted yarns by leveraging internal stress generated during the twisting process.

Optimal performance was achieved using 1 wt.% MXene ink and 20 wt.% CB-doped nanofibers. The conductive CB-doped TPU nanofibers bridged propagating cracks within the MXene coating, forming a synergetic conductive network that significantly improved the yarn's tensile sensing linearity from 0.810 to 0.994. The resulting yarn exhibited a broad sensing range of 106%, high sensitivity (GF = 56), slight mechanical hysteresis and stress softening, minimal static and dynamic drift, and a rapid response time (180 ms stretching and 230 ms releasing).

The combination of the self-shrunk scroll and double-twisted yarn structures establishes a dual-stage pressure-sensitive framework. Along with the enhanced conductivity from the synergistic network, this design enabled an ultrahigh pressure-sensing range of up to 10 MPa, with a linearity of 0.997 and sensitivity of 17.74 MPa^{-1} (0–3 MPa). The yarn also demonstrated exceptional durability, enduring over 5000 tensile and pressure cycles, and retained functionality after more than 30 ultrasonic washing cycles.

Practical demonstrations were demonstrated through smart textiles integrated with a single MXene@CB/TPU yarn, which effectively monitored tensile signals from joint bending, heartbeat, and respiration, as well as pressure signals from finger presses and footsteps. A smart lumbar support belt incorporating the yarn successfully detected dynamic pressure changes during physical activities and static pressure variations resulting from different sitting postures, highlighting its potential for real-world health monitoring and rehabilitation support.

Electronic Supplementary Material: Supplementary material (atomic force microscopy, X-ray diffraction patterns, scanning electron microscopy, water contact angles, resistivity measurements, and photographs and schematic diagram of samples) is available in the online version of this article at https://doi.org/10.26599/NR.2026.94908397.

Data availability

All data needed to support the conclusions in the paper are presented in the manuscript and the Electronic Supplementary Material. Additional data related to this paper may be requested from the corresponding author upon request.

Acknowledgements

This work is granted by the Zhejiang Provincial Postdoctoral Research Fund (No. ZJ2025031), the Zhejiang Provincial Natural Science Foundation of China (No. LR26E050002), the National Natural Science Foundation of China (No. U25A20321), the China Postdoctoral Science Foundation (No. 2025M770668), the Jiangsu Funding Program for Excellent Postdoctoral Talent, and the Zhiyuan Laboratory (ZYL2025005).

Declaration of competing interest

All the contributing authors report no conflict of interests in this work.

Author contribution statement

J. T.: Conceptualization, investigation, writing – original draft. H. L.: Investigation. Y. T. W.: Supervision, writing – review & editing. F. M.: Project administration. J. Z. Z.: Conceptualization. K. A. S. U.: Conceptualization. S. D. M.: Investigation. T. Y.: Conceptualization. Z. J. P.: Supervision. C. Y. X.: Data curation, validation. H. B. X.: Supervision. K. C. X.: Supervision, writing – review & editing. X. G. W.: Writing – review & editing. J. M. R.: Supervision, project administration, writing – review & editing. All the authors have approved the final manuscript.

Use of AI statement

None.

References

[1] Kim, K. H.; Kim, J. H.; Ko, Y. J.; Lee, H. E. Body-attachable multifunctional electronic skins for bio-signal monitoring and therapeutic applications. *Soft Sci.* **2024**, *4*, 24.

[2] Hou, Y. Y.; Xu, Y. H.; Cai, Z. M.; Wu, H.; Li, Y. B.; Shen, Z. C.; Xie, H. B.; Xu, K. C. Decoupled approaches for multimodal flexible sensor systems. *Nano Res.* **2025**, *18*, 94907673.

[3] Kwak, W.; Yin, J. Y.; Wang, S. L.; Chen, J. Advances in triboelectric nanogenerators for self-powered wearable respiratory monitoring. *FlexMat* **2024**, *1*, 5–22.

[4] Xu, Y. H.; Li, T. Y.; Zhou, H.; Lu, Y. Y.; Yuan, Y. Y.; Zhao, B. H.; Wang, Y. F.; Yang, H. Y.; Cai, X. J.; Nan, K. W. et al. A self-powered bioelectronic suture via hybrid laser treatment. *Adv. Healthc. Mater.* **2025**, *14*, 2501329.

[5] Kong, D. P.; Lu, Y. Y.; Zhou, S. Y.; Wang, M. K.; Pang, G. Y.; Wang, B. C.; Chen, L. P.; Huang, X. Y.; Lyu, H.; Xu, K. C. et al. Super-resolution tactile sensor arrays with sparse units enabled by deep learning. *Sci. Adv.* **2025**, *11*, eadv2124.

[6] Sheng, F. F.; Zhao, C.; Zhang, B.; Tan, Y. X.; Dong, K. Flourishing electronic textiles towards pervasive, personalized and intelligent healthcare. *Soft Sci.* **2024**, *4*, 2.

[7] Cai, Z. M.; Ye, K. J.; Luo, H. Y.; Tang, J.; Yang, G.; Xie, H. B.; Yang, H. Y.; Xu, K. C. Textile hybrid electronics for multifunctional wearable integrated systems. *Research* **2025**, *8*, 0779.

[8] Ma, S. D.; Wu, Y. T.; Tang, J.; Fu, J. Y.; Liu, H.; Zhang, Y. M.; Ma, J. Y.; Pan, Z. J.; Yan, T. Digitally interactive smart textiles in football prepared by an outstanding viscose-based flexible strain sensor. *Chem. Eng. J.* **2025**, *515*, 163421.

[9] Luo, H. Y.; Yang, G.; Jin, Z. G.; Cai, Z. M.; Li, Y. B.; Lu, Y. Y.; Wang, J.; Yang, H. Y.; Zheng, Y. F.; Xu, K. C. Textile hybrid electronics for monolithically multimodal wearable monitoring and therapy. *Int. J. Extrem. Manuf.* **2025**, *7*, 035506.

[10] Pu, J. H.; Ma, K. M.; Luo, Y. H.; Tang, S. Y.; Liu, T. Y.; Liu, J.; Leung, M.; Yang, J.; Hui, R. M.; Xiong, Y. et al. Textile electronics for wearable applications. *Int. J. Extrem. Manuf.* **2023**, *5*, 042007.

[11] Tang, J.; Wu, Y. T.; Ma, S. D.; Yan, T.; Pan, Z. J. Sensing mechanism of a flexible strain sensor developed directly using electrospun composite nanofiber yarn with ternary carbon nanomaterials. *iScience* **2022**, *25*, 105162.
[12] Tang, J.; Wu, Y. T.; Ma, S. D.; Yan, T.; Pan, Z. J. Strain-sensing composite nanofiber filament and regulation mechanism of shoulder peaks based on carbon nanomaterial dispersion. *ACS Appl. Mater. Interfaces* **2023**, *15*, 7392–7404.
[13] Liu, X. H.; Miao, J. L.; Fan, Q.; Zhang, W. X.; Zuo, X. W.; Tian, M. W.; Zhu, S. F.; Zhang, X. J.; Qu, L. J. Recent progress on smart fiber and textile based wearable strain sensors: Materials, fabrications and applications. *Adv. Fiber Mater.* **2022**, *4*, 361–389.
[14] Liu, Z. K.; Zhu, T. X.; Wang, J. R.; Zheng, Z. J.; Li, Y.; Li, J. S.; Lai, Y. K. Functionalized fiber-based strain sensors: Pathway to next-generation wearable electronics. *Nano-Micro Lett.* **2022**, *14*, 61.
[15] Wang, H. Y.; Wu, H.; Ye, D.; Zhao, C. Y.; Wu, Q. S.; Wang, S.; Zhang, Z. W.; Zeng, M. T.; Wei, H. H.; Huang, Y. A. Micro-cylindrical/fibric electronic devices: Materials, fabrication, health and environmental monitoring. *Soft Sci.* **2024**, *4*, 41.
[16] Tang, J.; Wu, Y. T.; Ma, S. D.; Yan, T.; Pan, Z. J. Flexible strain sensor based on CNT/TPU composite nanofiber yarn for smart sports bandage. *Compos. Part B: Eng.* **2022**, *232*, 109605.
[17] Wu, Y. T.; Tang, J.; Ma, S. D.; Zhang, K. Q.; Yan, T.; Pan, Z. J. A review of flexible strain sensors based on natural fiber materials. *Adv. Mater. Technol.* **2023**, *8*, 2201503.
[18] Wang, J. L.; Lu, C. H.; Zhang, K. Textile-based strain sensor for human motion detection. *Energy Environ. Mater.* **2020**, *3*, 80–100.
[19] Seyedin, S.; Zhang, P.; Naebe, M.; Qin, S.; Chen, J.; Wang, X. G.; Razal, J. M. Textile strain sensors: A review of the fabrication technologies, performance evaluation and applications. *Mater. Horiz.* **2019**, *6*, 219–249.
[20] Li, X. T.; Koh, K. H.; Farhan, M.; Lai, K. W. C. An ultraflexible polyurethane yarn-based wearable strain sensor with a polydimethylsiloxane infiltrated multilayer sheath for smart textiles. *Nanoscale* **2020**, *12*, 4110–4118.
[21] Chen, Y.; Zhang, Y. Y.; Song, F.; Zhang, H. Y.; Zhang, Q. K.; Xu, J.; Wang, H. P.; Ke, F. Y. Graphene decorated fiber for wearable strain sensor with high sensitivity at tiny strain. *Adv. Mater. Technol.* **2021**, *6*, 2100421.
[22] Zhang, S. C.; Sun, Y.; Xu, J. T. (3-Mercaptopropyl)triethoxysilane-modified reduced graphene oxide-modified polyurethane yarn enhanced by epoxy/thiol reactions for strain sensors. *ACS Appl. Mater. Interfaces* **2021**, *13*, 34865–34876.
[23] Xu, Y. M.; Xie, X. X.; Huang, H.; Wang, Y.; Yu, J. R.; Hu, Z. M. Encapsulated core–sheath carbon nanotube-graphene/polyurethane composite fiber for highly stable, stretchable, and sensitive strain sensor. *J. Mater. Sci.* **2021**, *56*, 2296–2310.
[24] Cai, R. M.; Liang, C. M.; Duan, Y. Q.; Zhao, Z. J.; Zhang, X.; He, P.; Yang, J. L.; Lai, W. Y.; Wei, J.; Tian, L. Metallic nanoparticle inks for flexible printed electronics. *FlexMat* **2025**, *2*, 225–283.
[25] Zhou, X. H.; Wang, Z.; Xiong, T.; He, B.; Wang, Z. X.; Zhang, H. Z.; Hu, D. M.; Liu, Y. T.; Yang, C. L.; Li, Q. W. et al. Fiber crossbars: An emerging architecture of smart electronic textiles. *Adv. Mater.* **2023**, *35*, 2300576.
[26] Dai, Y. L.; Qi, K.; Ou, K. K.; Song, Y. T.; Zhou, Y. M.; Zhou, M. L.; Song, H. J.; He, J. X.; Wang, H. B.; Wang, R. W. Ag NW-embedded coaxial nanofiber-coated yarns with high stretchability and sensitivity for wearable multi-sensing textiles. *ACS Appl. Mater. Interfaces* **2023**, *15*, 11244–11258.
[27] Qi, K.; Zhou, Y. M.; Ou, K. K.; Dai, Y. L.; You, X. L.; Wang, H. B.; He, J. X.; Qin, X. H.; Wang, R. W. Weavable and stretchable piezoresistive carbon nanotubes-embedded nanofiber sensing yarns for highly sensitive and multimodal wearable textile sensor. *Carbon* **2020**, *170*, 464–476.
[28] Qi, K.; Wang, H. B.; You, X. L.; Tao, X. J.; Li, M. Y.; Zhou, Y. M.; Zhang, Y. M.; He, J. X.; Shao, W. L.; Cui, S. Z. Core–sheath nanofiber yarn for textile pressure sensor with high pressure sensitivity and spatial tactile acuity. *J. Colloid Interface Sci.* **2020**, *561*, 93–103.
[29] Tang, J.; Wu, Y. T.; Ma, S. D.; Zhang, Y. M.; Yan, T.; Pan, Z. J. Three-directional knitted fabric sensor made of elastic carbon-based nanofiber yarn with excellent tensile and pressure sensing performance. *Nano Energy* **2024**, *128*, 109801.
[30] Wu, Y. T.; Yan, T.; Zhang, K. Q.; Pan, Z. J. A hollow core–sheath composite fiber based on polyaniline/polyurethane: Preparation, properties, and multi-model strain sensing performance. *Adv. Mater. Technol.* **2023**, *8*, 2200777.
[31] Zhou, B. Z.; Li, C. C.; Liu, Z. X.; Zhang, X. F.; Li, Q.; He, H. T.; Zhou, Y. F.; Jiang, L. A highly sensitive and flexible strain sensor based on dopamine-modified electrospun styrene-ethylene-butylene-styrene block copolymer yarns and multi walled carbon nanotubes. *Polymers* **2022**, *14*, 3030.
[32] Li, X. Q.; Li, X. K.; Wang, M. J.; Zheng, R. Q.; Jin, Y.; Gu, Z. J. Flexible and strain conductive cotton yarn enabled by low-temperature sintering of silver paste with multifunctional sensing capability in human motion detection and wearable applications. *Chem. Eng. J.* **2023**, *471*, 144843.
[33] Dou, L.; Zheng, X. H.; Yuan, M.; Li, D. Q.; Zhao, Z.; Tang, W. Y.; Fu, C.; Xia, Z. G.; Cai, G. M. Hierarchical and coaxial yarn with combined conductance stability and sensing capability for wearable electronics. *Appl. Mater. Today* **2022**, *29*, 101695.
[34] Usman, K. A. S.; Yao, Y.; Bacal, C. J. O.; Zhang, J. Z.; Jarvis, K. L.; Lynch, P. A.; Mota-Santiago, P.; Qin, S.; Naebe, M.; Henderson, L. C. et al. Robust biocompatible fibers from silk fibroin coated MXene sheets. *Adv. Mater. Interfaces* **2023**, *10*, 2201634.
[35] Usman, K. A. S.; Bacal, C. J. O.; Zhang, J. Z.; Qin, S.; Lynch, P. A.; Mota-Santiago, P.; Naebe, M.; Henderson, L. C.; Hegh, D. Y.; Razal, J. M. Tough and fatigue resistant cellulose nanocrystal stitched $Ti_3C_2T_x$ MXene films. *Macromol. Rapid Commun.* **2022**, *43*, 2200114.
[36] Usman, K. A. S.; Zhang, J. Z.; Hegh, D. Y.; Rashed, A. O.; Jiang, D. G.; Lynch, P. A.; Mota-Santiago, P.; Jarvis, K. L.; Qin, S.; Prime, E. L. et al. Sequentially bridged $Ti_3C_2T_x$ MXene sheets for high performance applications. *Adv. Mater. Interfaces* **2021**, *8*, 2002043.
[37] Zhou, K.; Guo, C. S.; Gan, F.; Xin, J. H.; Yu, H. Large-area ultra-thin GO nanofiltration membranes prepared by a pre-crosslinking rod coating technique. *J. Colloid Interface Sci.* **2023**, *640*, 261–269.
[38] Liu, Z. Y.; Zhao, L. H.; Ye, H. X.; Wang, Z. Y.; Chen, Y. H.; Li, Y. X.; Liu, L. P.; Guo, Y. L.; Chen, Y.; Niu, Q. J. Highly anions-selective polyamide nanofiltration membrane fabricated by rod-coating assisted interfacial polymerization. *J. Membr. Sci.* **2023**, *668*, 121273.
[39] Zhang, X. M.; Yang, X. L.; Wang, B. Highly stretchable, sensitive, and flexible strain sensors based on Ag@Cu/PDMS composites. *J. Mater. Sci.: Mater. Electron.* **2022**, *33*, 8104–8113.
[40] Gao, Y.; Guo, F. Y.; Cao, P.; Liu, J. C.; Li, D. M.; Wu, J.; Wang, N.; Su, Y. W.; Zhao, Y. Winding-locked carbon nanotubes/polymer nanofibers helical yarn for ultrastretchable conductor and strain sensor. *ACS Nano* **2020**, *14*, 3442–3450.
[41] Chen, L.; Mei, S. Q.; Fu, K.; Zhou, J. Spinning the future: The convergence of nanofiber technologies and yarn fabrication. *ACS Nano* **2024**, *18*, 15358–15386.
[42] Zhou, X.; Fang, S. L.; Leng, X. Q.; Liu, Z. F.; Baughman, R. H. The power of fiber twist. *Acc. Chem. Res.* **2021**, *54*, 2624–2636.
[43] Zhang, J. Z.; Kong, N.; Uzun, S.; Levitt, A.; Seyedin, S.; Lynch, P. A.; Qin, S.; Han, M. K.; Yang, W. R.; Liu, J. Q. et al. Scalable manufacturing of free-standing, strong $Ti_3C_2T_x$ MXene films with outstanding conductivity. *Adv. Mater.* **2023**, *32*, 2001093.
[44] Bu, Y. B.; Shen, T. Y.; Yang, W. K.; Yang, S. Y.; Zhao, Y.; Liu, H.; Zheng, Y. J.; Liu, C. T.; Shen, C. Y. Ultrasensitive strain sensor based on superhydrophobic microcracked conductive $Ti_3C_2T_x$ MXene/paper for human-motion monitoring and E-skin. *Sci. Bull.* **2021**, *66*, 1849–1857.

[45] Li, Q. M.; Yin, R.; Zhang, D. B.; Liu, H.; Chen, X. Y.; Zheng, Y. J.; Guo, Z. H.; Liu, C. T.; Shen, C. Y. Flexible conductive MXene/cellulose nanocrystal coated nonwoven fabrics for tunable wearable strain/pressure sensors. *J. Mater. Chem. A* **2020**, *8*, 21131–21141.

[46] Jia, Z. X.; Li, Z. J.; Ma, S. F.; Zhang, W. Q.; Chen, Y. J.; Luo, Y. F.; Jia, D. M.; Zhong, B. C.; Razal, J. M.; Wang, X. G. et al. Constructing conductive titanium carbide nanosheet (MXene) network on polyurethane/polyacrylonitrile fibre framework for flexible strain sensor. *J. Colloid Interface Sci.* **2021**, *584*, 1–10.

[47] Ma, S. D.; Tang, J.; Yan, T.; Pan, Z. J. Performance of flexible strain sensors with different transition mechanisms: A review. *IEEE Sens. J.* **2022**, *22*, 7475–7498.

[48] Pu, J. H.; Zhao, X.; Zha, X. J.; Li, W. D.; Ke, K.; Bao, R. Y.; Liu, Z. Y.; Yang, M. B.; Yang, W. A strain localization directed crack control strategy for designing MXene-based customizable sensitivity and sensing range strain sensors for full-range human motion monitoring. *Nano Energy* **2020**, *74*, 104814.

[49] Guo, X. H.; Zhao, Y. N.; Xu, X.; Chen, D. L.; Zhang, X. Y.; Yang, G.; Qiao, W.; Feng, R.; Zhang, X. Q.; Wu, J. et al. Biomimetic flexible strain sensor with high linearity using double conducting layers. *Compos. Sci. Technol.* **2021**, *213*, 108908.

[50] Wu, H. S.; Wang, C.; Liu, L. P.; Liu, Z. L.; He, J. H.; Zhang, C. C.; Duan, J. A. Bioinspired stretchable strain sensor with high linearity and superhydrophobicity for underwater applications. *Adv. Funct. Mater.* **2025**, *35*, 2413552.

[51] Mousavi, S.; Thai, M. T.; Amjadi, M.; Howard, D.; Peng, S. H.; Do, T. N.; Wang, C. H. Unidirectional, highly linear strain sensors with thickness-engineered conductive films for precision control of soft machines. *J. Mater. Chem. A* **2022**, *10*, 13673–13684.

[52] Huang, F.; Hu, J. Y.; Yan, X. A wide-linear-range and low-hysteresis resistive strain sensor made of double-threaded conductive yarn for human movement detection. *J. Mater. Sci. Technol.* **2024**, *172*, 202–212.

[53] Liu, B. Y.; Lan, B. X.; Shi, L. J.; Cheng, Y.; Sun, J.; Wang, R. R. Batch fabrication of flexible strain sensors with high linearity and low hysteresis for health monitoring and motion detection. *ACS Appl. Mater. Interfaces* **2024**, *16*, 36821–36831.

[54] Qi, X. M.; Wang, W. J.; Dai, H. B.; Zhu, Y. F.; Dong, Y. B.; Fu, S. Y.; Ni, Q. Q.; Fu, Y. Q. Multifunctional two-way shape memory RGO/ethylene-vinyl acetate composite yarns for electro-driven actuators and high sensitivity strain sensors. *Compos. Part A: Appl. Sci. Manuf.* **2023**, *169*, 107521.

[55] Zhang, Z. F.; Liu, S.; Wu, M. M.; Liu, S. Shape-adaptable and wearable strain sensor based on braided auxetic yarns for monitoring large human motions. *Appl. Mater. Today* **2023**, *35*, 101996.

[56] Wang, S. L.; Zhang, Z. Y.; Wang, R.; Jiang, X. J.; Gao, H. Y.; Xu, S.; Jamaluddin, N.; Qian, C.; Fu, Y. Q.; Dong, Y. B. PBAT/CNTs/PBAT yarn strain sensor with fully degradable, thermal repair, acid and alkali resistance, and waterproof functions. *Sustain. Mater. Technol.* **2025**, *43*, e01306.

[57] Yu, Q. H.; Pan, J. J.; Jiang, Z. H.; Guo, Z. G.; Jiang, J. H. Stretchable multimodal textile sensor based on core–sheath CB/PDMS/MXene sensing yarn for efficiently distinguishing mechanical stimulus. *Chem. Eng. J.* **2024**, *493*, 152462.

[58] Xin, Y. Y.; Zhou, J.; Tao, R.; Xu, X. Z.; Lubineau, G. Making a bilateral compression/tension sensor by pre-stretching open-crack networks in carbon nanotube papers. *ACS Appl. Mater. Interfaces* **2018**, *10*, 33507–33515.

[59] Zhang, X. Y.; Hu, Z. Y.; Sun, Q.; Liang, X.; Gu, P. Z.; Huang, J.; Zu, G. Q. Bioinspired gradient stretchable aerogels for ultrabroad-range-response pressure-sensitive wearable electronics and high-efficient separators. *Angew. Chem., Int. Ed.* **2023**, *62*, e202213952.

[60] Holm, R. *Electric Contacts: Theory and Application*; 4th ed. Springer: Berlin, 1967.

[61] Tang, J.; Wu, Y. T.; Ma, S. D.; Zhang, Y. M.; Xu, R. J.; Yan, T.; Pan, Z. J. Fabricating a smart clothing system based on strain-sensing yarn and novel stitching technology for health monitoring. *Sci. China Technol. Sci.* **2024**, *67*, 587–596.

[62] Munoz, F.; Rougier, P. R. Estimation of centre of gravity movements in sitting posture: Application to trunk backward tilt. *J. Biomech.* **2011**, *44*, 1771–1775.

[63] Wilke, H. J.; Neef, P.; Hinz, B.; Seidel, H.; Claes, L. Intradiscal pressure together with anthropometric data—A data set for the validation of models. *Clin. Biomech.* **2001**, *16*, S111–S126.

This is an open access article under the terms of the Creative Commons Attribution 4.0 International License (CC BY 4.0, https://creativecommons.org/licenses/by/4.0/).

© The Author(s) 2026. Published by Tsinghua University Press.